



Correction algorithm of the frequency-modulated continuous-wave LIDAR ranging system

XINYU CAO,¹ PING SONG,^{1,*} ZHIKANG PAN,² AND BOHU LIU¹

¹School of Mechatronical Engineering, Beijing Institute of Technology, Beijing 100081, China

²Beijing Information Science and Technology University, Beijing 100192, China

*spring2002@bit.edu.cn

Abstract: Frequency-modulated continuous-wave LIDAR has broad application prospects. Compared with the traditional pulse LIDAR, the FMCW LIDAR has the advantages of high resolution and long measurement distance. But it still can be affected by several factors, including environmental noise, spectrum aliasing, spectrum leakage and other issues. Some traditional filtering algorithms or signal transformation algorithms can improve the above problems, but the effect is not ideal. This paper proposes a signal correction algorithm called the VMD-based refined cross-power spectral density algorithm (VRCPSD). This algorithm is based on signal decomposition denoising and improved spectrum refinement methods. The algorithm applies variational mode decomposition, spectrum refinement and cross-power spectral density to signal processing. The VRCPSD algorithm is compared with the traditional spectrum correction algorithm on the high-speed linear array APD FMCW LIDAR experimental platform. The results show that the VRCPSD algorithm has a better spectrum correction effect on the LIDAR experimental platform. This algorithm can reduce the margin of error to the centimeter level. Therefore, the algorithm is promising in that it can improve the signal waveform of the FMCW laser radar ranging system, make the spectrum get better correction and make the distance more accurate.

© 2021 Optical Society of America under the terms of the [OSA Open Access Publishing Agreement](#)

1. Introduction

FMCW LIDAR ranging system has the advantages of broad measurement range, high range resolution, low peak power, simple hardware processing and low cost. It is a widely used ranging method with no blind zone theoretically [1].

FMCW LIDAR uses chirp signal as detection signal. The chirp signal is divided by an optical splitter, one of which is used as the local vibration signal, and the other is illuminated to the target surface as the detection signal by an optical collimation system. The reflected light signal of the target to be measured is received by the optical collimation system. After a series of processing, it is transmitted into the photoelectric detector for mixing to get beat signal. Finally, the signal processing system extracts the target distance information from the photocurrent signal. Therefore, the accuracy of FMCW ranging system is highly dependent on the signal resolution of the beat signal [1–3].

The intermediate frequency (IF) signal [4] is generated by mixing the transmitted signal and the received signal, and the corresponding beat signal spectrum can be obtained by fast fourier transform (FFT) [5]. In the actual measurement process, the hardware and the environment will produce much noise, which will affect the received echo signal [6]. At the same time, in order to balance the need for sampling and processing speed, the number of sampling points cannot be increased infinitely to meet requirements. Therefore, it is necessary to process the beat signal, not only to filter out the influence of noise, but also to obtain more precise spectral peaks, so

as to obtain the target distance more accurately. In order to achieve the above objectives, it is necessary to do noise reduction and spectral refinement of the signal.

In terms of noise reduction, the classical filtering method is to establish the correlation between time domain and frequency domain based on FFT. According to the relative distribution of signal and noise in the frequency domain, a low-pass filter is designed to filter the signal to eliminate high frequency noise. However, the classical filtering method is mainly used in stationary signals, and the denoising effect is more obvious when the distribution difference between signal and noise in the frequency domain is very significant [7]. Most of the LIDAR modulation signals are wide bandwidth and non-stationary [8]. The frequency function of the signal changes with time, and the classical filtering method is difficult to achieve a good denoising effect. Modern filtering methods mainly use some estimation algorithms to estimate useful signals from signals containing noise, or use the statistical characteristics of signals to filter out noise. Kalman filtering [9], Wiener filtering [10], particle filtering [11] and adaptive filtering [12] are widely used.

The noise reduction algorithm based on wavelet transform [13] is widely used in signal transform noise reduction methods. Different from FFT, wavelet transform (WT) has the characteristics of multi-resolution analysis, so WT is more suitable for analyzing non-stationary signals. However, WT is extremely dependent on the types of basis functions and threshold settings, and cannot adaptively decompose different signals [14].

Signal decomposition noise reduction methods mainly include noise reduction method based on independent component analysis (ICA) [15], noise reduction method based on singular value decomposition (SVD) [16], noise reduction method based on sparse decomposition and noise reduction method based on empirical mode decomposition (EMD) [17]. In the process of noise reduction, these methods involve decomposing the input signal and analyzing the decomposed signal components to remove the noise components one by one [3].

The traditional method to improve the frequency resolution is to increase the number of sampling points, zeroing after the sampling data [18]. However, this method requires to truncate the time-domain signal first, which is equivalent to adding a rectangular window. It will cause spectrum leakage very seriously. In theory, there can be no leakage provided that the intercept time is equal to an integral multiple of the frequency component cycle. However, for the unknown signal analyzed, it is impossible to ensure that the sampling frequency is the integral multiple of the spectrum of each frequency component, and that the intercept length is exactly equal to the integral multiple of the cycle of each frequency component. Moreover, in order to improve the spectrum density, zero-filling operation is necessary, so the spectrum leakage is inevitable.

Zoom-FFT (ZFFT) is called a refined fast Fourier transform [19]. The function of ZFFT is local refinement and amplification of the signal frequency, which is convenient for analysis. The essence of ZFFT is to transform a wideband signal into a narrowband signal through a band-pass filter, so that the sampling frequency can be reduced by resampling, and then a fewer point FFT can be used to achieve higher frequency resolution. However, in fact, although ZFFT is often called a spectrum refining algorithm, it cannot improve the frequency resolution as it only selects the frequency band we care about to calculate [20]. For us, we can also directly figure out FFT spectrum and only draw the band we care about. Compared with the direct FFT method, ZFFT has no increase in the information obtained [19]. It only improves the calculation efficiency. It is more appropriate to be called belt selection analysis.

Chirp-z transform (CZT) was proposed by Lawrence Rabiner when analyzing speech signals in 1968 [21], which can turn the unit circle of the z plane into a spiral gradually from the unit origin to the unit circle. This algorithm can improve the frequency resolution, and can arbitrarily choose the starting frequency and calculation interval. CZT can greatly improve the frequency resolution, which is one of the classical algorithms of spectrum refinement. The only drawback is that CZT has little effect on solving spectrum leakage [22], and it is difficult to determine the true signal spectrum peak in many spectrum peaks.

In view of the problems such as large noise influence, low frequency resolution and spectrum leakage in the traditional algorithm for signal processing, an improved spectral peak correction algorithm based on signal decomposition is proposed. Our main contribution are summarized as follows:

1. Effectively reduce the influence of high frequency noise on acquisition signal. In the signal decomposition transform part, the signal is decomposed into k narrowband AM-FM signals under the condition of preset scale k [23]. This is an adaptive time-frequency analysis method, which can effectively deal with non-stationary signals and suppress noise from the environment and hardware only by selecting the appropriate k value. At the same time, this algorithm can effectively suppress the modal aliasing effect. After the intrinsic mode functions obtained after decomposition are restored by the correlation coefficient method, the time-domain acquisition data after noise reduction can be obtained, used as the input of the next level of processing.
2. Effectively improve the frequency resolution. In the spectral peak correction part, the CZT algorithm is used to refine the spectrum of the data collected by the FMCW system [24]. Under the condition that the hardware sampling rate and the number of sampling points are restricted, the position of the spectral peak is more accurate, and the accuracy of the system ranging is improved.
3. Effectively judge the real spectrum peak to avoid the misjudgment caused by spectrum leakage. Since the signal collected in one measurement is multi-cycle, the cross-power spectral density (CPSD) can be calculated by refining the spectrum to locate the spectral peak range of each cycle. CPSD is a modal parameter frequency domain identification method, which is initially based on the peak value of the natural frequency of the structure in its frequency response function [25]. The peak value becomes a good estimation of the characteristic frequency. In the FMCW LIDAR ranging system, the frequency-domain characteristics of signal energy concentration can be effectively obtained, so as to accurately locate the spectral peak and ignore the influence of the secondary peak caused by spectrum leakage [26].

The principle of FMCW LIDAR ranging system is briefly analyzed in Sect. 2, and the principle of VRCPSD algorithm is theoretically introduced in Sect. 3. The effect of the VRCPSD algorithm is separately evaluated and compared by simulation and experimental analysis in Sects. 4 and 5. Finally, the conclusions are presented in Sect. 6.

2. Sixteen-channel FMCW LIDAR ranging system

Figure 1 is the schematic diagram of FMCW LIDAR ranging system. First of all, the remote computer sends out instructions to make the signal processing module of the system control the frequency modulation continuous wave signal generator to produce the FMCW laser driving signal, which drives the continuous wave laser tube to emit laser, and then the transmitted laser is shaped by the linear laser emission system, so that the transmitted laser is linearly illuminated to the target surface. The target reflected light converges to the photosensitive surface of 16*1 linear array avalanche photodiode (APD) through the sector field of view receiving optical system [27], and is converted into 16 channels of receiving signals carrying target information. After receiving signals are grouped, continuous IF signals are obtained by synchronous amplification, mixing, filtering and automatic gain processing of multiple dual-channel synchronous mixer modules. The IF signal is sampled at high speed by the parallel analog-digital (AD) sampling module and transmitted to the signal processing control module. After the acquisition process is completed, the linear APD LIDAR is uploaded to the host computer through the communication-level

synchronous control interface, and the distance information of the target is calculated by the spectral characteristics of the IF signal.

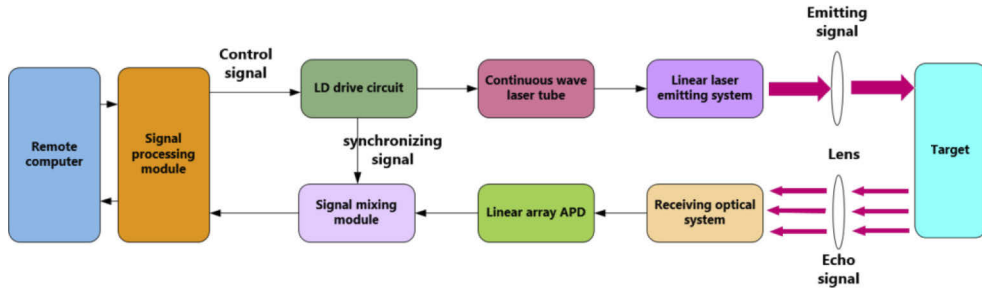


Fig. 1. FMCW LIDAR ranging system

The emission signal $s_e(t)$ and receiving signal $s_r(t)$ in a modulation period can be calculated by the following Eq. (1).

$$\begin{cases} s_e(t) = A_0 \cos [2\pi(f_0 t + \frac{1}{2}\mu t^2) + \phi_0], & t \in [0, T] \\ s_r(t) = K_r A_0 \cos \{2\pi [f_0(t - \tau(t)) + \frac{1}{2}\mu(t - \tau(t))^2] + \phi_0 + \varphi_0\} \end{cases} \quad (1)$$

where A_0 is the amplitude of the emission signal, f_0 is the initial modulation frequency, B is the modulation bandwidth, ϕ is the initial phase of emission signal, μ is the modulation slope. Due to the use of sawtooth wave frequency modulation, $\mu = B/T$ in the modulation cycle. T is the time of one modulation cycle, τ is time delay. K_r is the decay coefficient related to target reflection intensity etc. φ_0 is the additional phase shift caused by target reflection. After frequency mixing, IF Signal $s_{IF}(t)$ and the spectrum $S_{IF}(f)$ can be calculated by Eq. (2).

$$\begin{cases} s_{IF}(t) = \frac{1}{2} K_r A_0^2 \cos \left[2\pi \left(\frac{2\mu R - 2f_0 v_0}{c} t + \frac{2f_0 R}{c} \right) - \varphi_0 \right] \\ S_{IF}(f) = \frac{1}{2} K_r A_0^2 \exp \left[j \left(\frac{4\pi f_0 R}{c} - \varphi_0 \right) \right] \cdot TSa \left[\pi \left(f - \frac{2\mu R}{c} + \frac{2f_0 v_0}{c} \right) T \right] \end{cases} \quad (2)$$

c is the light velocity, R is the detecting distance, v_0 is the relative velocity. Select the highest spectrum peak according to the distribution of spectrum, target distance can be calculated by

$$R = \frac{Tc}{2B} f_{IF} \quad (3)$$

f_{IF} is the frequency corresponding to the highest peak. The minimum distinguishable distance of the system is calculated by Eq. (4).

$$\Delta R = \frac{Tc}{2B} \Delta f_{IF} \quad (4)$$

Δf_{IF} is the frequency resolution of IF signal. By Eq. (4), the minimum resolution of the system is only related to Δf_{IF} . Therefore, how to improve the frequency resolution will be the most important work in this paper. The signal processing algorithm is introduced in detail in Sect. 3.

3. VRCPSD algorithm processing

VRCPSD algorithm is a high efficient signal processing method for FMCW LIDAR ranging system. The schematic diagram of this algorithm is shown as Fig. 2.

The detailed description of this algorithm is as follows

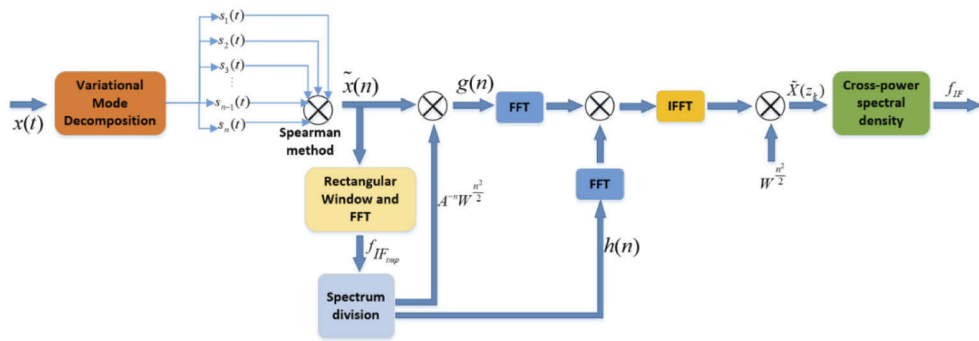


Fig. 2. Diagram of the VRCPSD algorithm

1. Decompose the multi-component echo signal into several signal components with practical physical significance by variational mode decomposition (VMD), and restore the signal by spearman correlation coefficient method [28].
2. Process the restored signal by rectangular window and FFT transform to obtain the spectrum of the signal and the maximum peak position of each cycle without refinement.
3. Select the refined bandwidth range by taking the unrefined maximum spectral peak position obtained in the second step as the center, and refine the spectrum by CZT method.
4. Divide the signals of 20 cycles collected at a time into 10 groups. The cross-power spectrum density of each group of signals is calculated to obtain 10 groups of peaks [25]. Find the maximum value of the 10 groups of peaks. The frequency corresponding to the maximum peak is f_{IF} . Therefore the measurement distance can be calculated.

Compared with EMD, which has drawbacks including endpoint effect, modal overlap, susceptible to noise, etc. VMD has prominent advantages in processing non-stationary signals and suppressing noise [23]. By reasonably setting the preset scale k , VMD can also effectively suppress modal aliasing.

VMD decomposes the original signal into n intrinsic mode functions (IMFs) with limited bandwidth expressed as Eq. (5):

$$s_n(t) = A_n(t) \cos(\omega_n(t)). \quad (5)$$

$s_n(t)$ is the IMF n , $A_n(t)$ is the instantaneous amplitude and $\omega_n(t)$ is the instantaneous frequency. Each IMF concentrates at central frequency, thus bandwidth can be calculated by Eq. (6):

$$\left\{ \begin{array}{l} \min_{\{s_n\}, \{\omega_n\}} = \left\{ \sum \left\| \partial t \left[\left(\sigma(t) + \frac{j}{\pi t} \right) s_n(t) \right] e^{i-j\omega_n t} \right\|_2^2 \right\} \\ \sum_{n=1}^N s_n = x(t) \end{array} \right. . \quad (6)$$

Introduce augmented Lagrangian function for optimal solution.

$$\begin{aligned} L(\{s_n\}, \{\omega_n\}, \lambda) = & a \sum_n \left\| \partial t \left[\left(\sigma(t) + \frac{j}{\pi t} \right) s_n(t) \right] e^{i-j\omega_n t} \right\|_2^2 \\ & + \left\| x(t) - \sum_n s_n(t) \right\|_2^2 + \left\langle \lambda(t), x(t) - \sum_n s_n(t) \right\rangle \end{aligned} \quad (7)$$

In Eq. (7), α is the penalty factor which affects the accuracy of decomposition and λ is the lagrangian multiplier. The process of VMD is as follows.

1. Initialize $\{s_n\}$, $\{\omega_n\}$, λ_1 and n to 0.
2. Start loop iteration after $m = m + 1$.
3. Increase n from $n + 1$ to N . Update s_n^{m+1} , ω_n^{m+1} and λ as follows

$$\begin{aligned} S_n^{m+1}(\omega) &\leftarrow \frac{X(\omega) - \sum_{i \neq n} S_i(\omega) + \frac{\Lambda(\omega)}{2}}{1 + 2\alpha(\omega - \omega_n^m)^2} \\ \omega_n^{m+1} &\leftarrow \frac{0}{\int_0^\infty |\omega| S_n^{m+1}(\omega)^2 d\omega} \\ \Lambda^{m+1}(\omega) &\leftarrow \Lambda^m(\omega) + \gamma \left(X(\omega) - \sum_n S_n^{m+1}(\omega) \right) \end{aligned} \quad (8)$$

γ is noise tolerance to meet the fidelity requirement of signal decomposition. $S_n^{m+1}(\omega)$, $S_i(\omega)$, $X(\omega)$, $\Lambda(\omega)$ correspond to Fourier Transform of $s_n^{m+1}(t)$, $s_i(t)$, $x(t)$, $\lambda(t)$.

4. Repeat step.3, the condition for stopping iteration is showed by Eq. (9).

$$\sum_n \|s_n^{m+1} - s_n^m\|_2^2 / \|s_n^m\|_2^2 < \epsilon \quad (9)$$

For this FMCW system, the decomposition effect is best when $k = 5$. The decomposed IMFs are restored by Spearman method, and the problems such as spectrum aliasing and spectrum leakage are effectively avoided.

The finite length sequence obtained after processing is denoted by $\tilde{x}(n)$. Its z-transform can be calculated by Eq. (10):

$$\tilde{X}(z) = \sum_{n=0}^{N-1} \tilde{x}(n) z^{-n}. \quad (10)$$

For the CZT transformation, the value can be taken along a more general path in the z plane. Therefore, a section of bare line in the z plane is sampled with equal angle, and the sampling point is calculated by

$$z_k = AW^{-k}, k = 0, 1, \dots, M-1, \quad (11)$$

where M is the number of points for analysis, which is not necessarily equal to N . $f_{IF_{tmp}}$, which is the frequency corresponding to the maximum spectral peak before spectrum refinement, can be calculated by FFT, thus required parameters of CZT can be obtained.

$$\begin{aligned} f_1 &= f_{IF_{tmp}} - 0.5F_b \\ f_2 &= f_{IF_{tmp}} + 0.5F_b \\ A &= \exp(1i * 2\pi f_1 / F_s) \\ W &= \exp(-1i * 2\pi(f_2 - f_1) / (F_s * M_b)) \end{aligned} \quad (12)$$

where F_b is the refined bandwidth, F_s is sampling frequency, M_b is the number of points in refined frequency bands. CZT of $\tilde{x}(n)$ can be calculated by Eq. (13),

$$\begin{aligned} \tilde{X}(z_k) &= \sum_n \tilde{x}(n) (AW^{-k})^{-n} \\ &= W^{\frac{k^2}{2}} \sum_n g(n) h(k-n) \\ &= W^{\frac{k^2}{2}} g(k) * h(k), k = 0, 1, \dots, N-1 \end{aligned} \quad (13)$$

where

$$\begin{aligned} g(n) &= \tilde{x}(n)A^{-n}W^{\frac{n^2}{2}}, n = 0, 1, \dots, N-1 \\ h(n) &= W^{-\frac{n^2}{2}} \end{aligned} . \quad (14)$$

$\tilde{X}(z_k)$ is the refined spectrum of beat frequency signal in one cycle. There are 20 cycles in one acquisition. Each cycle corresponding to a CZT transformation can be denoted as

$$\tilde{X}_i(z_k), i = 1, 2, \dots, 20. \quad (15)$$

The spectrum resolution has been greatly improved by CZT refinement method. To further distinguish the spectral peaks of real echo signals, CPSD of signal is needed.

CPSD represents the power density distribution of the signal in the frequency domain, and the result indicates that the energy of the target echo is relatively concentrated in a certain frequency. Therefore, f_{IF} can be regarded as the frequency corresponding to the maximum peak value of CPSD. In order to prevent the impact of short-term signal mutation and improve stability and reliability of the algorithm, CPSD is performed between each two cycles. For the multi-cycle signals collected, the CPSD flow diagram is shown as Fig. 3.

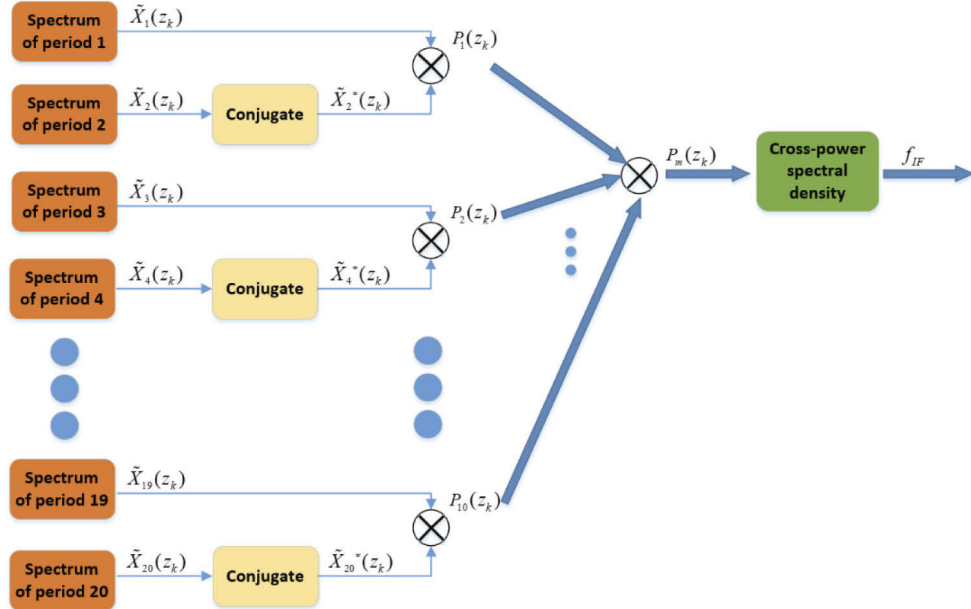


Fig. 3. Diagram of CPSD processing

where

$$P_m(Z_k) = \max\{P_i(Z_k)\}, i = 1, 2, \dots, 20. \quad (16)$$

CPSD represents the power density distribution of beat signals in the frequency domain. The energy of the target echo is relatively concentrated at a certain frequency. Therefore, the maximum value of CPSD can be regarded as where the degree of signal correlation reaches the highest. Taking the corresponding frequency value as f_{IF} , the interference can be reduced as much as possible to obtain a more accurate distance value. According to Eq. (3), target distance can be calculated finally. CPSD can find the real peak of the signal more accurately, and the spectrum peak in the spectrum is likely to be covered by the interference spectrum peak, which

cannot well reflect the power distribution of the signal. So this step plays an important role in VRCPSD algorithm.

To evaluate the performance of VRCPSD algorithm, SNR [29] is adapted as a performance index, which can be calculated by Eq. (17). Signals can be constructed by IFFT after processing.

$$SNR = 10\log_{10} \left[\frac{\max\{|\tilde{X}_i(z_k)|^2\}}{|P_m(Z_k)^2| - \max\{|\tilde{X}_i(z_k)|^2\}} \right] \quad (17)$$

In Table 1, f_L and f_U represent lower cut-off frequency and upper cut-off frequency respectively. These two parameters are decided by the performance of low pass filter in the experimental platform and the parameter T . They determine the upper and lower limits of measuring distance.

Table 1. Simulation and experiment parameters

| Parameter | Value | Parameter | Value |
|-----------|--------------|------------|---------|
| c | 299792458m/s | F_s | 250MHz |
| λ | 808nm | F_B | 1000Hz |
| T | 100μs | R_{\min} | 2.0m |
| B | 100MHz | R_{\max} | 16.0m |
| f_L | 10kHz | A_0 | 1 |
| f_U | 150kHz | μ | 1MHz/μs |

In Sects. 4 and 5, the performance of the proposed VRCPSD algorithm is evaluated by both simulation and practical experiment.

4. Simulation results

The effect of VRCPSD algorithm can be evaluated by MATLAB simulation. Other signal correction algorithm, such as FFT, EMD, VMD and CZT are also investigated to compare with the performance of VRCPSD algorithm. By giving the same input signal, the spectral characteristics and SNR are compared.

For EMD, the parameter of k is determined by the decomposition stop criteria. Set maximum number of extrema in the residual signal as 1. EMD stops when the number of extrema is less than maximum number of extrema. In this paper, the parameter k of EMD is 7.

For VMD, the parameter of k is manually set before decomposition. The selection of k value adopts the maximum kurtosis principle. Increase k from 1, and then calculate the kurtosis of the IMF with the largest correlation coefficient at each k value. When the kurtosis reaches its maximum, the corresponding k value is required. In this paper, the parameter k of VMD is 4.

Because that IF signal is composed of emission signal and echo signal, it is presented as beat signal. Therefore, set beat frequency signal as input signal of VRCPSD algorithm. Noise is also added to the signal. Results of simulation are shown on Fig. 4.

In Fig. 4, while the images of FFT and CZT are beat signal after IFFT of corresponding spectrum, the images of the other three methods are not simply obtained by IFFT. For EMD and VMD method, the left images are obtained by reconstructing IMFs by Spearman rank correlation coefficient method. For VRCPSD method, the power spectrum is obtained from the power spectrum density, and then the spectrum is constructed from the power spectrum. Thus IFFT is calculated to get the left image. As is shown, FFT method still retains a lot of noise from the original signal. The principle of EMD algorithm is to use the extreme value of the signal to fit the envelope of the signal with the interpolation method and perform recursive decomposition. Because of the uneven distribution of local extremum, the envelope signal destroys the integrity of the original signal, resulting in a large error in IMF decomposition. Therefore, the signal curve

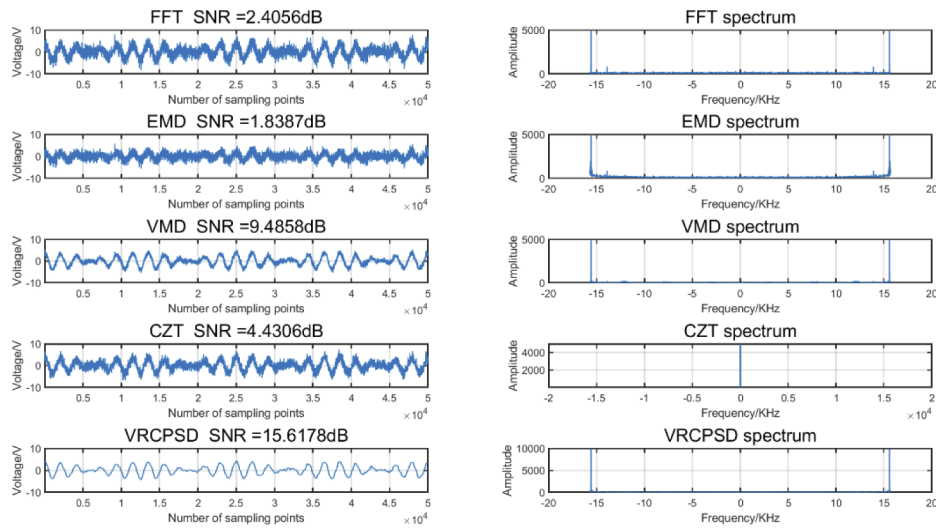


Fig. 4. Results of different methods in simulation

after denoising has a certain peak distortion. Moreover, this method requires accurate parameters such as threshold. If the threshold setting is not correct, EMD algorithm cannot completely remove the high-frequency components in the noise signal, but reduces the SNR of the signal. In VMD algorithm, since the defined IMF is narrow-band, the effect of removing high-frequency noise is much better than that of EMD algorithm. It can also be seen in Fig. 4 that the SNR of the signal processed by VMD method has been greatly improved. However, VMD algorithm has some spectrum leakage in the decomposition process, which will produce some frequency components that do not exist and cause some interference to spectrum analysis. CZT algorithm can refine the spectrum, so that the information of the spectrum is more abundant and complete. But for a whole signal, CZT has little help in denoising. It is more useful for the detailed analysis of a certain signal. It can also be seen from the Fig. 4 that CZT is not very helpful for improving SNR of the original signal.

In the VRCPSD algorithm, it can be seen that this algorithm not only has signal decomposition and spectrum refinement, but also calculates the cross-power spectral density of signals with different cycles, so it improves the ratio of target spectral peak to interference spectral peak. Therefore, VRCPSD algorithm has the best SNR and is clearer when determining the key parameter f_{IF} .

Compared with the simulation results of the above algorithms, the advantages of VRCPSD algorithm are very obvious, which greatly improves the signal SNR and accurately restores the spectral peak where the signal energy concentrates. In Sect. 5, detailed experiment is applied to show the performance of several algorithms in practical use.

5. Experimental results

In order to evaluate the performance of VRCPSD algorithm for distance calculation of FMCW LIDAR ranging system, this paper presents the hardware design of this system, and gives the performance of VRCPSD algorithm in signal processing. At the same time, other algorithms are also experimentally investigated to compare with this algorithm.

Figure 5 shows the diagram of the experimental prototype. Considering the influence of ambient light, vapor and smoke in the air, a relatively good SNR can be obtained by selecting a longer wavelength laser emitter [30]. Considering the technical maturity, volume, cost and

power characteristics of the laser diode, the laser diode with a wavelength of 808 nm and a power of 1.2W is used in the hardware design of this system. The diode is driven by the FM signal generated by the dual-channel DDS chip AD9958BCPZ. The laser is reflected on the target, and focused on the APD to generate echo signal. The echo signal is weak, so it needs to be amplified by the amplifier circuit AD8001. On the other hand, the local oscillator signal and the emission signal are synchronized through the synchronous signal, and the echo signal is mixed with the mixer AD831 to form the beat signal. The beat signal contains the sum and difference of the spectral components of the emission signal and the echo signal, and the sum of the frequency components is a high-frequency interference signal without information. Therefore, it is necessary to filter out the signal through the low-pass filter MAX274, and then amplify it through the amplifier circuit AD8002 to obtain the IF signal with an appropriate amplitude. The IF signal is sampled by AD9253 with sampling frequency of 20 MHz, and transmitted to FPGA ZYNQ7100 for temporary storage, and then transmitted to PC via TCP/IP protocol for subsequent algorithm solution.

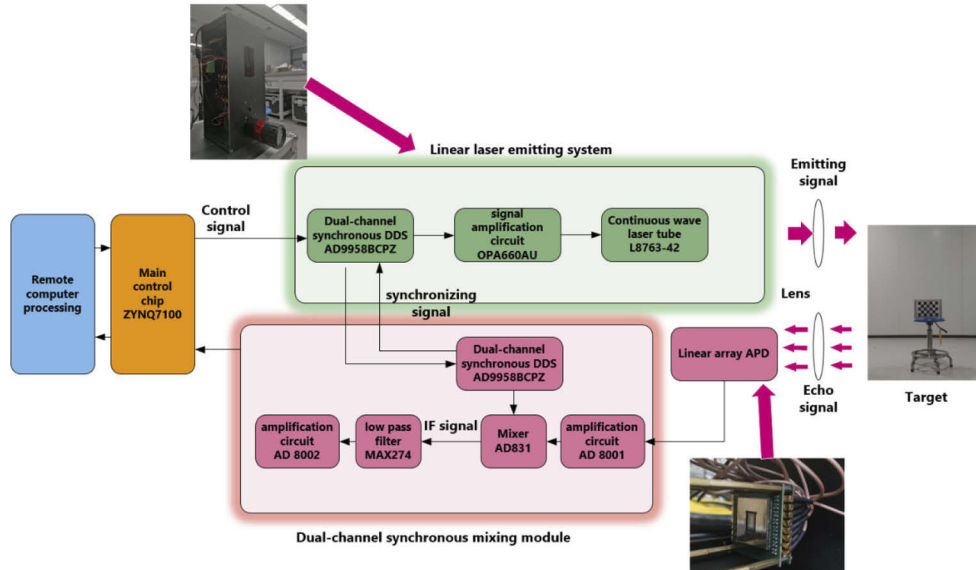


Fig. 5. Diagram of experimental prototype

During the experiment, in order to better test the ranging accuracy of the FMCW LIDAR ranging system under different distances, the experimental platform is arranged as follows.

The platform is placed in a straight line with the target. According to Eq. (3), considering f_L and f_U , the lower limit and upper limit of distance ought to be 1.499m and 22.484m. Therefore, change the distance between the target and the linear array APD from 2 to 16 m with a step of 0.1m.

To visually show the processing effect of VRCPSD algorithm on waveform in practical experiments, several echo signals measured at integer points are selected and processed by this algorithm. Figure 6 presents the echo signals and processed signals at 2,4,6,8,10,12,14,16 meters.

It can be seen from the preliminary experimental results in Fig. 6 that the VRCPSD algorithm has greatly improved measured echo signals. Signals before processing have peak distortion [31] and saw-tooth distortion with many burrs in the waveform. After processed by VRCPSD algorithm, waveforms are smoother and more regular, and there is no obvious waveform distortion. In order to further investigate the improvement of VRCPSD algorithm on the FMCW LIDAR ranging performance, several algorithms in the simulation are applied to process the actual

experimental echo signal, and the Sum of Squared Error (SSE), Mean Square Error (MSE), Mean Absolute Error (MAE), Mean Absolute Percentage Error (MAPE), Root Mean Square Error (RMSE) after different algorithms are calculated [32], so as to compare the performance of different algorithms. Figures 7–11 shows the specific ranging errors of various algorithms.

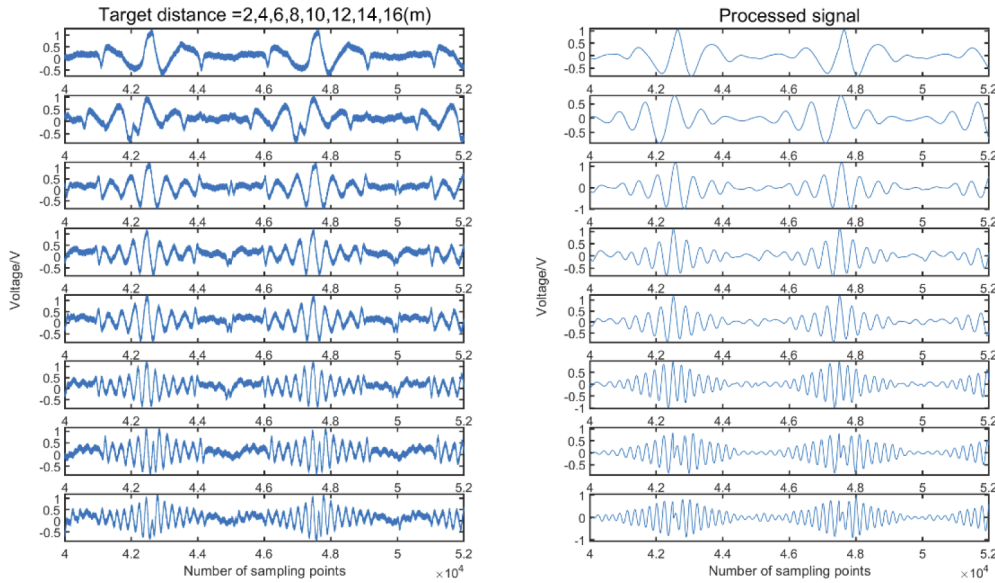


Fig. 6. Echo signals and processed signals at several meters.

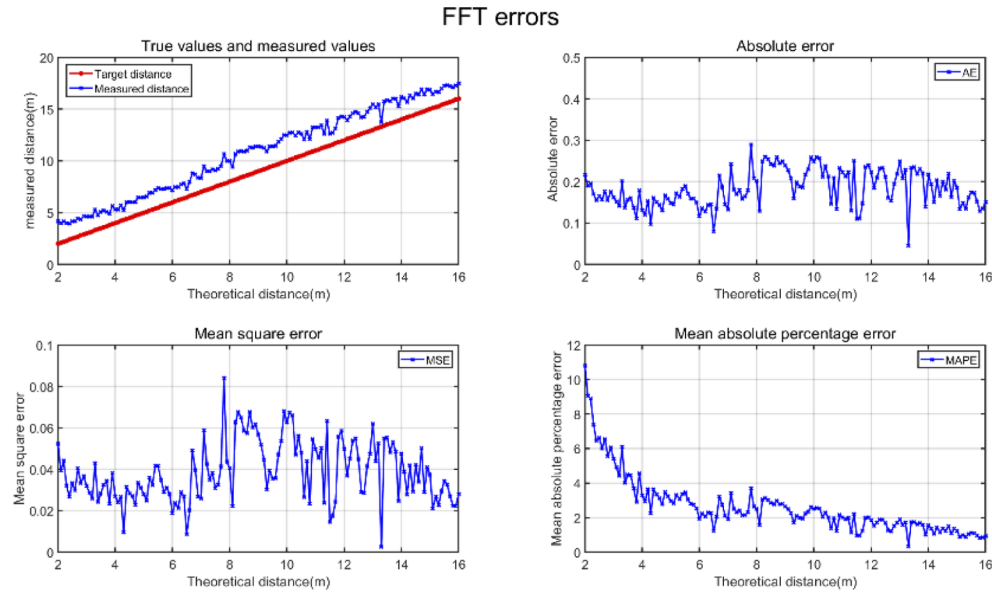
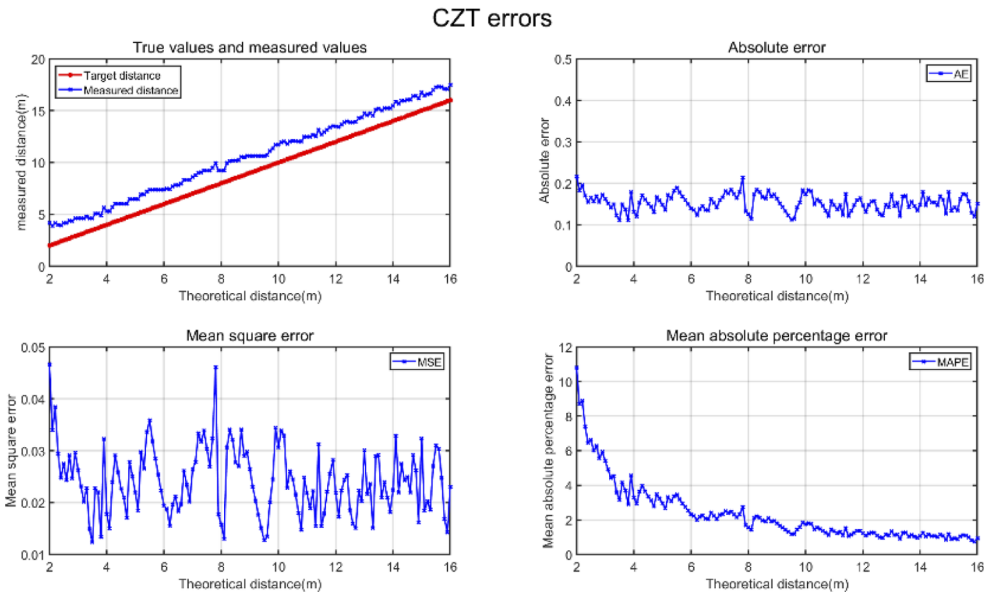
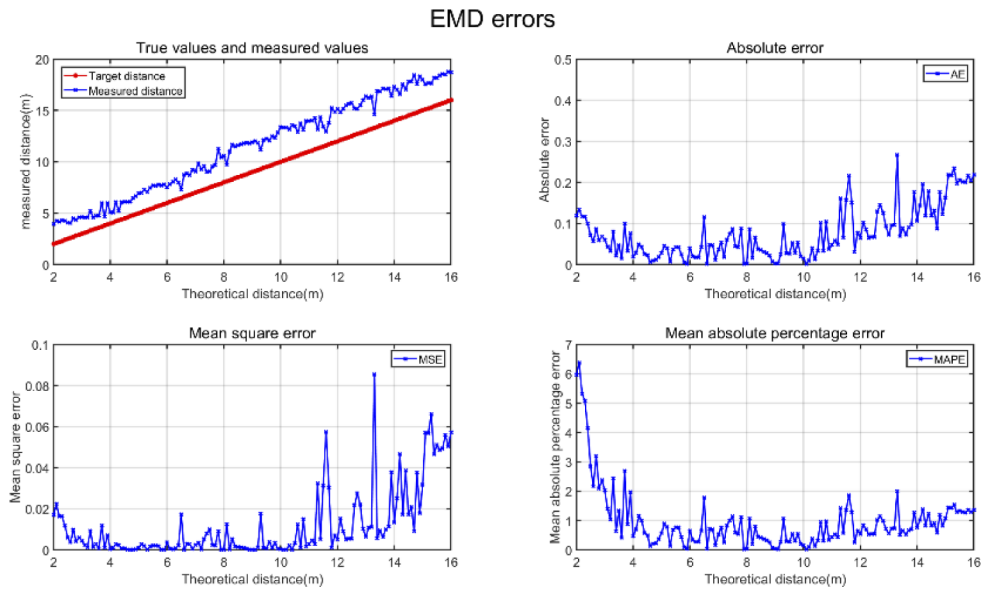
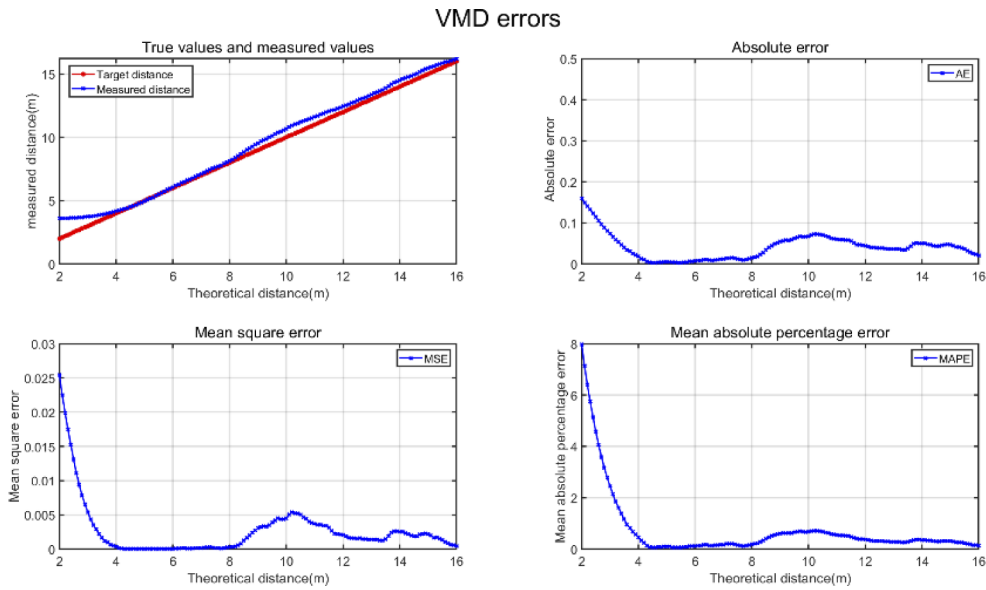
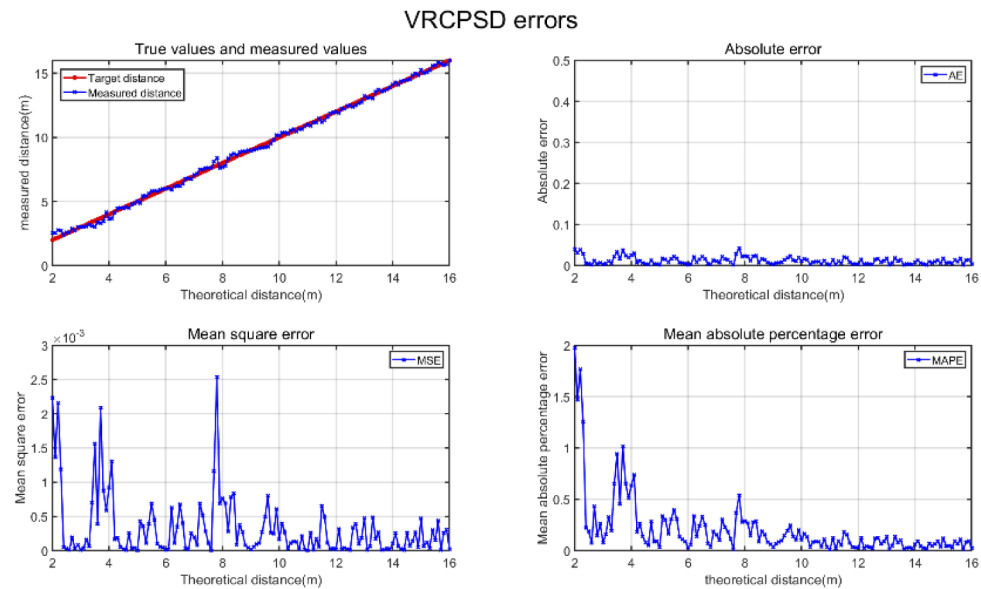


Fig. 7. Specific ranging errors of FFT algorithm

As is shown in Fig. 7–11, VRCPSD has the best spectrum correction and ranging performance, while other algorithms have a large gap between the object distance and the real distance. From the absolute error diagram of each algorithm, it can be seen that the errors of FFT, CZT, EMD

**Fig. 8.** Specific ranging errors of CZT algorithm**Fig. 9.** Specific ranging errors of EMD algorithm

**Fig. 10.** Specific ranging errors of VMD algorithm**Fig. 11.** Specific ranging errors of VRCPSD algorithm

and VMD algorithms are at the decimeter level, and the maximum error will reach above 20 centimeters. The error of VRCPSD algorithm is concentrated in about one centimeter, and the maximum error is less than 5 cm. SSE, MSE, MAPE, RMSE also have better performance than other algorithms. In order to compare the ranging errors of each algorithm more clearly, their absolute errors are compared in Fig. 12, and their maximum, minimum and average errors are compared in Table 2.

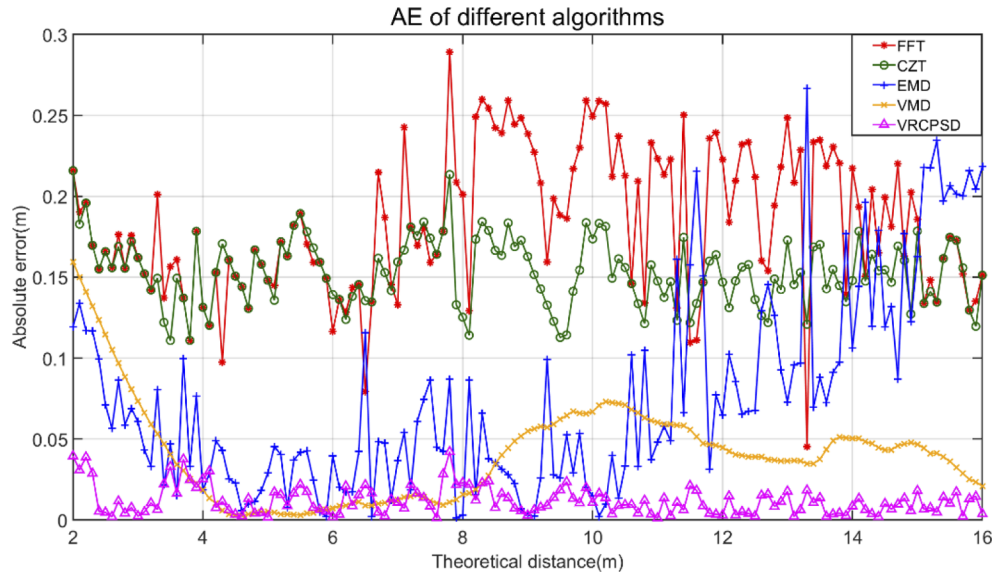


Fig. 12. Absolute errors of different algorithms

Table 2. Maximum, minimum and average absolute errors of different algorithms

| Algorithm | FFT | CZT | EMD | VMD | VRCPSD |
|---------------|---------|---------|---------|---------|---------|
| Maximum AE(m) | 0.28913 | 0.21586 | 0.26673 | 0.15936 | 0.04209 |
| Minimum AE(m) | 0.04519 | 0.11091 | 0.00128 | 0.00302 | 0.00189 |
| Mean AE(m) | 0.18274 | 0.15331 | 0.07546 | 0.04110 | 0.01188 |

As is shown in Fig. 12 and listed in Table 2, the ranging results of echo signal from 2m to 16m show that the maximum absolute error has been reduced from 0.28913m of FFT to 0.04209m of VRCPSD, and the average error has also been reduced from 0.18274m to 0.01188m. MAPE is also reduced from 10.793% to 1.975%. The overall offset error of an algorithm can be replaced by the average absolute error at each measurement point after simple simplification. That is to say, the VRCPSD algorithm not only has smaller deviation, but also has smaller offset error than other algorithms. Based on the comparison that are shown in Fig. 7–12 and Table 2, it can be found that the VRCPSD algorithm provides a better performance than the other methods in FMCW LIDAR ranging. Meanwhile, the time required for processing the same signal under the same initial conditions with different algorithms is shown in Table 3. The time cost of VRCPSD algorithm is obviously higher than other algorithms, which is one of the future optimization directions.

The ranging accuracy is determined by the echo signal and the hardware parameters of the system. Therefore, in order to obtain the ideal ranging performance of the system, there are some requirements for the hardware besides the improvement of the signal processing algorithm.

Table 3. Signal processing time of different algorithms

| Algorithm | FFT | CZT | EMD | VMD | VRCPSD |
|---------------------|--------|--------|--------|--------|--------|
| Processing time (s) | 1.2587 | 1.6972 | 1.6099 | 1.9091 | 3.5416 |

For example, the selected laser power should not be too low, otherwise the echo signal is too weak to be covered by the ambient light, and the ideal beat signal may not be obtained after mixing. Sampling accuracy of ADC should be greater than 12 bits in order to get enough signal resolution. In this experiment, a laser diode with 1.2w and a 14-bit ADC are used to meet the demands. However, by increasing the laser power and the number of bits of the ADC, better results can still be obtained. In addition, the performance of the system can be improved by selecting high multiple amplifiers, lifting mixers and improving low-pass filters [33].

6. Conclusion

An algorithm applied for FMCW LIDAR ranging system is proposed and verified by simulation and experiment. Compared with traditional denoising methods including FFT, CZT, EMD and VMD, VRCPSD algorithm not only reduces the influence of noise on echo signal, but also refines the spectrum and improves the frequency resolution. Besides, this algorithm also determines the concentration of energy in time domain, completely getting rid of interference peaks from spectrum leakage. In the experimental environment, MAPE is reduced from a maximum of 10.793% to 1.975%, and AE is reduced to less than 0.05m with a MAE as low as 0.01188m. Above all, VRCPSD algorithm is extremely helpful in improving the range resolution of FMCW LIDAR ranging system. In future study, it is necessary to upgrade hardware systems to adapt to more complex environments and thus, enhance the performance of the system under various conditions.

Funding. National Defense Basic Scientific Research Program of China (JCKY2019602B010).

Acknowledgments. The authors wish to thank the editor and the anonymous reviewers for their valuable suggestions.

Disclosures. The authors declare no conflicts of interest.

Data availability. Data underlying the results presented in this paper are not publicly available at this time but may be obtained from the authors upon reasonable request.

References

1. I. P. Hwang, S. J. Yun, and C. H. Lee, "Mutual Interferences in Frequency-Modulated Continuous-Wave (FMCW) LiDARs," *Optik* **220**, 165109 (2020).
2. F. G. Fernald, "Analysis of atmospheric lidar observations: some comments," *Appl. Opt.* **23**(5), 652–653 (1984).
3. P. Avishekha, C. Douglas C, S. Michael, and K. Dennis K, "Differential absorption lidar CO₂ laser system for remote sensing of TATP related gases," *Appl. Opt.* **48**(4), B145 (2009).
4. B. Journet and G. Bazin, "A low-cost laser range finder based on an FMCW-like method," *IEEE Trans. Instrum. Meas.* **49**(4), 840–843 (2000).
5. F. Millioz, "Sparse Detection in the Chirplet Transform: Application to FMCW Radar Signals," *IEEE Trans. Signal Process.* **60**(6), 2800–2813 (2012).
6. R. White P and J. Locke, "Performance of methods based on the fractional Fourier transform for the detection of linear frequency modulated signals," *IET Signal Process.* **6**(5), 478–483 (2012).
7. B. Liu, C. Song, and Y. Duan, "The characteristics simulation of FMCW laser backscattering signals," *Opt. Rev.* **25**(2), 197–204 (2018).
8. S. Pal, A. Behrendt, and V. Wulfmeyer, "Elastic-backscatter-lidar-based characterization of the convective boundary layer and investigation of related statistics," *Ann. Geophys.* **28**(3), 825–847 (2010).
9. R. Kalman, "A new approach to linear filtering and predicted problems," *J. Basic Eng.* **82**(1), 35–45 (1960).
10. P. Hoeher, "Two-dimensional pilot-symbol-aided channel estimation by Wiener filtering," at *1997 IEEE International Conference on Acoustics, Speech, and Signal Processing* (1997).
11. J Deutscher, A Blake, and I Reid, "Articulated body motion capture by annealed particle filtering," *Proceedings IEEE Conference on Computer Vision and Pattern Recognition. CVPR 2000 (Cat. No.PR00662)*. IEEE (2000).
12. S. P. Talebi, S. Werner, and D. P. Mandic, "Complex-Valued Nonlinear Adaptive Filters With Applications in α -Stable Environments," *IEEE Signal Process. Lett.* **26**(9), 1315–1319 (2019).

13. W. Boles W and B. Boashash, "A human identification technique using images of the iris and wavelet transform," *IEEE Trans. Signal Process.* **46**(4), 1185–1188 (1998).
14. Y. Xu, J. B. Weaver, D. M. Healy, and L. Jian, "Wavelet transform domain filters: a spatially selective noise filtration technique," *IEEE Trans. on Image Process.* **3**(6), 747–758 (1994).
15. A. Delorme and S. Makeig, "EEGLAB: an open source toolbox for analysis of single-trial EEG dynamics including independent component analysis," *J. Neurosci. Methods* **134**(1), 9–21 (2004).
16. O. Alter, O. Brown P, and D. Botstein, "Singular value decomposition for genome-wide expression data processing and modeling," *Proc. Natl. Acad. Sci. U. S. A.* **97**(18), 10101–10106 (2000).
17. J. C. Nunes, Y. Bouaoune, R. Deléchelle, O. Niang, and P. Bunel, "Image analysis by bidimensional empirical mode decomposition," *Image Vis. Comput.* **21**(12), 1019–1026 (2003).
18. J. Liu and H. Ying, "Zoom FFT Spectrum by Fourier Transform," *J. Vibr. Engin.* (1995).
19. C. Ma, Q. Zhou, J. Qin, W. L. Xie, Y. Dong, and W. S. Hu, "Fast Spectrum Analysis for an OFDR Using the FFT and SCZT Combination Approach," *IEEE Photonics Technol. Lett.* **28**(6), 657–660 (2016).
20. A. Khan N and B. Boashash, "Instantaneous Frequency Estimation of Multicomponent Nonstationary Signals Using Multiview Time-Frequency Distributions Based on the Adaptive Fractional Spectrogram," *IEEE Signal Process. Lett.* **20**(2), 157–160 (2013).
21. R. Rabiner L, W. Schafer R, and M. Rader C, "The chirp z-transform algorithm," *IEEE Trans. Audio Electroacoust.* **17**(2), 86–92 (1969).
22. T. Radil, M. Ramos P, and C. Serra A, "New Spectrum Leakage Correction Algorithm for Frequency Estimation of Power System Signals," *IEEE Trans. Instrum. Meas.* **58**(5), 1670–1679 (2009).
23. K. Dragomiretskiy and D. Zosso, "Variational Mode Decomposition," *IEEE Trans. Signal Process.* **62**(3), 531–544 (2014).
24. R. Tong and W. Cox R, "Rotation of NMR images using the 2D chirp-z transform," *Magn. Reson. Med.* **41**(2), 253–256 (1999).
25. X Zhang and J Ying, "A Soft Decision Based Noise Cross Power Spectral Density Estimation for Two-Microphone Speech Enhancement Systems," *IEEE International Conference on Acoustics. IEEE* (2005).
26. M A Damavandi and S Nader-Esfahani, "Compressive wideband spectrum sensing in cognitive radio systems using CPSD," *2015 International Conference on Communications, Signal Processing, and their Applications (ICCSA'15)*. IEEE (2015).
27. L. Thomas D and N. George, "Large-volume, low-cost, high-precision FMCW tomography using stitched DFBs," *Opt. Express* **26**(3), 2891 (2018).
28. C. Spearman, "The proof and measurement of association between two things," *Int. J. Epidemiol.* **39**(5), 1137–1150 (2010).
29. R. Tandra and A. Sahai, "SNR Walls for Signal Detection," *IEEE J. Sel. Top. Signal Process.* **2**(1), 4–17 (2008).
30. H. B. Yu, M. Chin, T. L. Yuan, H. S. Bian, L. A. Remer, J. M. Prospero, A. Omar, D. Winker, Y. K. Yang, Y. Zhang, Z. B. Zhang, and C. Zhao, "The Fertilizing Role of African Dust in the Amazon Rainforest: A First Multiyear Assessment Based on CALIPSO Lidar Observations," *Geophys. Res. Lett.* **42**(6), 1984–1991 (2015).
31. N. Dyson, "Peak distortion, data sampling errors and the integrator in the measurement of very narrow chromatographic peaks," *J. Chromatogr. A* **842**(1-2), 321–340 (1999).
32. R. F. Engle, "Cointegration and error correction: representation, estimation, and testing," *Econometrica* **55**, 251–276 (1987).
33. R. P. Basler, G. H. Price, R. T. Tsunoda, and T. L. Wong, "Ionospheric distortion of HF signals," *Radio Sci.* **23**(4), 569–579 (1988).